SCIENCE CHINA
Physics, Mechanics & Astronomy

• Article •

April 2016 Vol. 59 No. 4: 642002
doi: 10.1007/s11433-016-5781-0

# Theoretical study of fusion reactions $^{32}$S + $^{94,96}$Zr and $^{40}$Ca + $^{94,96}$Zr and quadrupole deformation of $^{94}$Zr†

Bing Wang[1], WeiJuan Zhao[1], EnGuang Zhao[2,3], and ShanGui Zhou[2,3*]

[1]*Department of Physics, Zhengzhou University, Zhengzhou 450001, China;*
[2]*State Key Laboratory of Theoretical Physics, Institute of Theoretical Physics, Chinese Academy of Sciences, Beijing 100190, China;*
[3]*Center of Theoretical Nuclear Physics, National Laboratory of Heavy Ion Accelerator, Lanzhou 730000, China*

Received October 24, 2015; accepted November 12, 2015; published online January 28, 2016

The dynamic coupling effects on fusion cross sections for reactions $^{32}$S + $^{94,96}$Zr and $^{40}$Ca + $^{94,96}$Zr are studied with the universal fusion function formalism and an empirical coupled channel (ECC) model. An examination of the reduced fusion functions shows that the total effect of couplings to inelastic excitations and neutron transfer channels on fusion in $^{32}$S + $^{94}$Zr ($^{40}$Ca + $^{94}$Zr) is almost the same as that in $^{32}$S + $^{96}$Zr ($^{40}$Ca + $^{96}$Zr). The enhancements of the fusion cross section at sub-barrier energies due to inelastic channel coupling and neutron transfer channel coupling are evaluated separately by using the ECC model. The results show that effect of couplings to inelastic excitations channels in the reactions with $^{94}$Zr as target should be similar as that in the reactions with $^{96}$Zr as target. This implies that the quadrupole deformation parameters $\beta_2$ of $^{94}$Zr and $^{96}$Zr should be similar to each other. However, $\beta_2$'s predicted from the finite-range droplet model, which are used in the ECC model, are quite different. Experiments on $^{48}$Ca + $^{94}$Zr or $^{36}$S + $^{94}$Zr are suggested to solve the puzzling issue concerning $\beta_2$ for $^{94}$Zr.

**empirical coupled channel model, barrier distribution, universal fusion function, neutron transfer**

**PACS number(s):** 24.10.-i, 25.60.Pj, 25.40.Hs, 25.70.Jj

**Citation:** B. Wang, W. J. Zhao, E. G. Zhao, and S. G. Zhou, Theoretical study of fusion reactions $^{32}$S + $^{94,96}$Zr and $^{40}$Ca + $^{94,96}$Zr and quadrupole deformation of $^{94}$Zr, Sci. China-Phys. Mech. Astron. **59**, 642002 (2016), doi: 10.1007/s11433-016-5781-0

## 1 Introduction

Heavy-ion fusion reaction has been an interesting topic for several decades because the heavy-ion fusion not only is of central importance for nucleosynthesis but also can reveal rich interplay between nuclear structure and reaction dynamics [1-7]. The study of fusion reaction mechanism is also of fundamental importance for understanding the synthesis of superheavy elements, properties of weakly bound nuclei, and symmetry energy of the nuclear equation of state [8-17]. Up to now, lots of important information about fusion dynamics at energies near the Coulomb barrier, especially at sub-barrier energies, are obtained through experimental and theoretical studies, such as the fusion hindrance phenomenon at extreme low energies—a steep falloff of the fusion cross sections [18-23], the role of the neutron transfer effect in the fusion [24-27], the breakup effect on the fusion reactions process [28-35], etc.

In the sub-barrier energy region, a large enhancement of fusion cross section for the fusion reaction of $^{58}$Ni + $^{64}$Ni as compared with that for $^{58}$Ni + $^{58}$Ni and $^{64}$Ni + $^{64}$Ni was observed by Beckerman et al. [28]. Broglia et al. [29, 30] suggested that the coupling to transfer channels with positive $Q$ values is needed to explain the enhancement of fusion data for the Ni + Ni systems. Large enhancements of sub-barrier fusion cross sections have been also observed in many other reaction systems with positive $Q$-value neutron transfer (PQNT) channels, such as the reaction systems $^{32}$S + $^{A}$Pd ($A$

*Corresponding author (email: sgzhou@itp.ac.cn)
†Contributed by ShanGui Zhou (Associate Editor)

= 104-106, 108, and 110) [36], $^{40}$Ca + $^{44,48}$Ca [37], $^{40}$Ca + $^{94,96}$Zr [38, 39], and $^{32}$S + $^{94,96}$Zr [40, 41]. For some of these systems, the fusion excitation functions have been measured in sufficiently small energy steps, which can be used to extract the underlying barrier distributions to study the contribution from transfer channels. The experimental barrier distributions are much broader than those of the reaction systems with negative $Q$-value neutron transfer channel. However, in some other experiments for reaction systems with PQNT channels [42, 43], no extra enhancement was observed in the fusion cross sections at sub-barrier energies.

Theoretically, many efforts have been made to understand the effect of the neutron transfer channels. In ref. [31], the authors proposed that a neutron flow between the projectile and the target nuclei before fusion could promote neck formation which provides a force strong enough to overcome the Coulomb force. Therefore the fusion is more favored and the sub-barrier fusion cross section is enhanced. In ref. [44], Zagrebaev proposed a simplified semiclassical model to describe the effect of neutron transfer on fusion. This effect depends on both neutron transfer probabilities and their $Q$ values. The PQNT provides a gain in the kinetic energy. Consequently, the fusion is easier and the sub-barrier fusion cross section is enhanced. Sargsyan et al. [45-47] suggested that the deformations of the interacting nuclei change owing to the PQNT. Thus, the influence of the PQNT channels on fusion is accompanied by and depends on the change of nuclear deformations. In the quantum coupled channel (QCC) model [48], the coupling to PQNT channels is treated approximately by using a macroscopic form factor. Within the microscopic dynamics models, such as the quantum molecular dynamic model [49-54] and the time-dependent Hartree-Fock method [55-61], the effects of surface excitations as well as nucleon transfer can be automatically included. Up to now, although many experiments and theoretical efforts have been devoted to study the mechanism of the coupling to PQNT channels, the underlying mechanism is still far from a clear understanding.

In our previous work [62], we have proposed an empirical coupled channel (ECC) model. In the ECC model, a barrier distribution is used to take effectively into account the effects of couplings. The effect of the coupling to PQNT channels is simulated by broadening the barrier distribution. The ECC model was also extended to include breakup effects [63]. In ref. [62], a systematic study of capture excitation functions for 217 reaction systems has been performed by using the ECC model. Among these 217 reaction systems, there are 86 systems with positive $Q$ values for one neutron pair transfer channel. The calculated capture cross sections of most of these 86 reaction systems are in good agreement with the experimental values, including $^{32}$S + $^{96}$Zr and $^{40}$Ca + $^{96}$Zr. However, the calculated results underestimate the sub-barrier cross sections for $^{32}$S + $^{94}$Zr and $^{40}$Ca + $^{94}$Zr. These results seem to be similar to those obtained from ref. [41]. In ref. [41], a large enhancement for the sub-barrier fusion cross sections was deduced in $^{32}$S + $^{94}$Zr compared to $^{32}$S + $^{96}$Zr based on QCC calculations without the neutron transfer effect considered, although the $Q(xn)$ values, which are listed in Table 1, for $^{32}$S + $^{94}$Zr are relatively smaller than those for $^{32}$S + $^{96}$Zr. The authors suggested that the neutron transfer effect in $^{32}$S + $^{94}$Zr are much stronger than that in $^{32}$S + $^{96}$Zr. In the present work, we will study the dynamic coupling effects in the reactions $^{32}$S + $^{94,96}$Zr and $^{40}$Ca + $^{94,96}$Zr with the universal fusion function (UFF) formalism and the ECC model. We will first investigate the dynamic coupling effects on fusion cross sections with the UFF formalism. Then, the effects of couplings to inelastic excitations and neutron transfer channels on fusion are analysed separately with the ECC model.

The present paper is organized as follows. In sect. 2, the ECC model is briefly reviewed. The method used to eliminate geometrical factors and static effects of the data is introduced in sect. 3 where the influence on fusion cross section owing to inelastic excitations and transfer couplings will be also investigated. A summary is given in sect. 4.

## 2 Methods

The fusion cross section at a given center-of-mass energy $E_{\rm c.m.}$ can be written as the sum of the cross section for each partial wave $J$,

$$\sigma_{\rm f}(E_{\rm c.m.}) = \frac{\pi\hbar^2}{2\mu E_{\rm c.m.}} \sum_{J}^{J_{\max}} (2J+1) T(E_{\rm c.m.}, J), \qquad (1)$$

here $\mu$ denotes the reduced mass of the reaction system and $T$ denotes the penetration probability. $J_{\max}$ is the critical angular momentum: For the partial wave with angular momentum larger than $J_{\max}$, the "pocket" of the interaction potential disappears. The interaction potential around the Coulomb barrier is approximated by an "inverted" parabola.

The couplings between the relative motion of the two nuclei and other degrees of freedom including the coupling to

**Table 1** $Q$ values for one or multineutron transfer channels from ground state to ground state for $^{32}$S + $^{90,94,96}$Zr, $^{36}$S + $^{94}$Zr, $^{40}$Ca + $^{90,94,96}$Zr, and $^{48}$Ca + $^{90,94,96}$Zr

| Reaction | $Q(1n)$ (MeV) | $Q(2n)$ (MeV) | $Q(3n)$ (MeV) | $Q(4n)$ (MeV) |
|---|---|---|---|---|
| $^{32}$S+$^{90}$Zr | −3.33 | −1.23 | −6.60 | −6.16 |
| $^{32}$S+$^{94}$Zr | 0.42 | 5.10 | 3.46 | 6.15 |
| $^{32}$S+$^{96}$Zr | 0.79 | 5.74 | 4.51 | 7.66 |
| $^{36}$S+$^{94}$Zr | −3.92 | −2.61 | −6.88 | −6.32 |
| $^{40}$Ca+$^{90}$Zr | −3.61 | −1.44 | −5.86 | −4.18 |
| $^{40}$Ca+$^{94}$Zr | 0.14 | 4.89 | 4.19 | 8.12 |
| $^{40}$Ca+$^{96}$Zr | 0.51 | 5.53 | 5.24 | 9.64 |
| $^{48}$Ca+$^{90}$Zr | −6.82 | −9.78 | −17.31 | −20.77 |
| $^{48}$Ca+$^{94}$Zr | −3.07 | −3.45 | −7.26 | −18.53 |
| $^{48}$Ca+$^{96}$Zr | −2.71 | −2.81 | −6.21 | −6.95 |

PQNT channels result in an enhancement in the fusion cross sections at sub-barrier energies. In the ECC model [62], a barrier distribution $f(B)$ is introduced to take into account the coupled channel effects in an empirical way. Then, the penetration probability is calculated as:

$$T(E_{\rm c.m.}, J) = \int f(B) T_{\rm HW}(E_{\rm c.m.}, J, B) {\rm d}B. \quad (2)$$

$T_{\rm HW}$ denotes the penetration probability calculated by the well-known Hill-Wheeler formula [64]. Note that for very deep sub-barrier penetration, the Hill-Wheeler formula is not valid because of the long tail in the Coulomb potential. In ref. [65], a new barrier penetration formula was proposed for potential barriers containing a long-range Coulomb interaction and this formula is especially appropriate for the barrier penetration with penetration energy much lower than the Coulomb barrier.

The barrier distribution $f(B)$ is taken to be an asymmetric Gaussian function

$$f(B) = \begin{cases} \dfrac{1}{N} \exp\left[-\left(\dfrac{B - B_{\rm m}}{\Delta_1}\right)^2\right], & B < B_{\rm m}, \\ \dfrac{1}{N} \exp\left[-\left(\dfrac{B - B_{\rm m}}{\Delta_2}\right)^2\right], & B > B_{\rm m}. \end{cases} \quad (3)$$

$f(B)$ satisfies the normalization condition $\int f(B){\rm d}B = 1$. $N = \sqrt{\pi}(\Delta_1 + \Delta_2)/2$ is a normalization coefficient. $\Delta_1$, $\Delta_2$, and $B_{\rm m}$ denote the left width, the right width, and the central value of the barrier distribution, respectively.

Within the ECC model [62], the barrier distribution is related to the couplings to low-lying collective vibrational states and rotational states. The vibrational modes are connected to the change of nuclear shape. Nuclear rotational states are related to static deformations of the interacting nuclei. Furthermore, when the two nuclei come close enough to each other, both nuclei are distorted owing to the attractive nuclear force and the repulsive Coulomb force, thus dynamical deformations develop [12, 44]. Considering the dynamical deformation, a two-dimensional potential energy surface (PES) with respect to relative distance $R$ and quadrupole deformation of the system can be obtained. Based on the PES, empirical formulas were proposed for calculating the parameters of the barrier distribution in ref. [62]. Note that such empirical formulas are connected with the quadrupole deformation parameters predicted by the finite-range droplet model (FRDM) [66].

The effect of the coupling to the PQNT channel is simulated by broadening the barrier distribution. Only one neutron pair transfer channels is considered in the ECC model. When the $Q$ value for one neutron pair transfer is positive, the widths of the barrier distribution are calculated as $\Delta_i \rightarrow fQ(2n) + \Delta_i, (i = 1, 2)$, where $Q(2n)$ is the $Q$ value for one neutron pair transfer. $f$ is taken as 0.32 for all reactions with positive $Q$ value for one neutron pair transfer channel [62].

## 3 Results and discussion

The fusion excitation function is influenced by two types of features related to the structure of and interaction potential between the projectile and the target. One is of a static nature, such as the heights, curvatures and radii of the barriers, and the static effects associated with the excess protons or neutrons in weakly bound nuclei. The other one is the dynamic effect of couplings to inelastic excitations, the breakup channel, and nucleon transfer channels. In order to study the dynamic coupling effects on fusion cross sections, it is necessary to eliminate the geometrical factors and static effects of the potential between the two nuclei [67, 68]. In the present work, we will first investigate the dynamic coupling effects on fusion cross sections by eliminating the static effects with the UFF formalism. Then, the effects of couplings to inelastic excitations and neutron transfer channels on fusion are analysed separately with the ECC model. Since $^{32}$S and $^{40}$Ca are both well bound, the breakup effects are not important.

### 3.1 Reduced fusion excitation functions

We adopt the method proposed in refs. [67, 68] to eliminate the geometrical factors and static effects of the potential between the two nuclei. According to this prescription, the fusion cross section and the collision energy are reduced to a dimensionless fusion function $F(x)$ and a dimensionless variable $x$,

$$F(x) = \frac{2E_{\rm c.m.}}{R_{\rm B}^2 \hbar\omega} \sigma_{\rm f}, \quad x = \frac{E_{\rm c.m.} - V_{\rm B}}{\hbar\omega}, \quad (4)$$

where $E_{\rm c.m.}$ is the collision energy in the center-of-mass frame, $\sigma_{\rm f}$ is the fusion cross section, and $V_{\rm B}$, $\hbar\omega$, and $R_{\rm B}$ denote the height, curvature, and radius of the barrier which is approximated by a parabola. The barrier parameters $V_{\rm B}$, $\hbar\omega$, and $R_{\rm B}$ are obtained from the double folding and parameter-free São Paulo potential (SPP) [70-72].

If the fusion cross section can be accurately described by the Wong's formula [73]

$$\sigma_{\rm f}^{\rm W}(E_{\rm c.m.}) = \frac{R_{\rm B}^2 \hbar\omega}{2E_{\rm c.m.}} \ln\left[1 + \exp\left(\frac{2\pi(E_{\rm c.m.} - V_{\rm B})}{\hbar\omega}\right)\right], \quad (5)$$

then $F(x)$ reduces to

$$F_0(x) = \ln\left[1 + \exp(2\pi x)\right], \quad (6)$$

which is called the universal fusion function (UFF) [67, 68]. Note that $F_0(x)$ is independent of reaction systems. So $F_0(x)$ is used as a uniform standard reference to explore the coupling effects on fusion cross sections. Deviations of the fusion function from the UFF, if exist, are assumed to mainly arise from the dynamic coupling effects on fusion cross section.

The reduced fusion excitation functions of the reactions $^{32}$S + $^{90,94,96}$Zr and $^{40}$Ca + $^{90,94,96}$Zr are shown in Figure 1. The solid lines represent the UFF. The parameters of the potential used in the reduction procedure are obtained from the

SPP and listed in Table 2. On one hand, the deviations of the reduced fusion excitation functions from the UFF for $^{32}$S + $^{90,94,96}$Zr and $^{40}$Ca + $^{90,94,96}$Zr are very large, especially for $^{32}$S + $^{94,96}$Zr and $^{40}$Ca + $^{94,96}$Zr. This implies that the enhancement of the sub-barrier cross sections due to the coupling effects in $^{32}$S, $^{40}$Ca + $^{94,96}$Zr are much larger than that in $^{32}$S,$^{40}$Ca + $^{90}$Zr. This is because that the neutron transfer channels are opened in $^{32}$S, $^{40}$Ca + $^{94,96}$Zr. The $Q(xn)$ values for the neutron transfer channels from ground state to ground state for $^{32}$S + $^{90,94,96}$Zr and $^{40}$Ca + $^{90,94,96}$Zr are shown in Table 1. On the other hand, the behaviors of the reduced fusion excitation functions of $^{32}$S + $^{94}$Zr and $^{32}$S + $^{96}$Zr are very similar. The situation is the same for the reactions $^{40}$Ca + $^{94,96}$Zr. This implies that the total effect of the couplings to inelastic excitations and neutron transfer channels in $^{32}$S + $^{94}$Zr ($^{40}$Ca + $^{94}$Zr) is almost the same as that in $^{32}$S + $^{96}$Zr ($^{40}$Ca + $^{96}$Zr).

It is well-known that the coupling to PQNT channels enhances the sub-barrier fusion cross section. However, a quantitative understanding of the enhancement due to PQNT channel coupling remains elusive because the only observable is the total enhancement of the cross section. In order to further understand the effect of the neutron transfer channels in these reactions, we will study the effects of couplings to inelastic excitations and neutron transfer channels on fusion separately by using the ECC model.

### 3.2 Couplings to inelastic excitations and PQNT channels

In this section, we will isolate the effect of transfer coupling from that of couplings to the inelastic excitations channels. We first estimate the enhancement due to inelastic excitations channel couplings alone by adopting the ECC model [62].

The experimental fusion excitation functions and the results from ECC calculations for $^{32}$S, $^{40,48}$Ca + $^{90}$Zr and $^{48}$Ca + $^{96}$Zr are shown in Figure 2. For these four reactions, the $Q$ values of neutron transfer are negative as seen in Table 1. Therefore, only the couplings to inelastic excitations channels are responsible for the enhancement. The solid lines denote the results from the ECC calculations. In the ECC calculations, the static quadrupole deformation parameters $\beta_2 = 0.035$, $\beta_2 = 0.062$, and $\beta_2 = 0.217$ are used for $^{90,94,96}$Zr [66], respectively. One can find that results from the ECC calculations are in good agreement with the data. This implies that the ECC model with the barrier distributions obtained from ref. [62] can describe well the effect of the couplings to inelastic excitations channels. Therefore, the ECC calculations can provide an accurate quantitative estimate of the enhancement due to inelastic excitations channel couplings alone.

As mentioned above, the sub-barrier cross section of reactions $^{32}$S + $^{94,96}$Zr ($^{40}$Ca + $^{94,96}$Zr) shows an extra enhancement as compared with that of $^{32}$S + $^{90}$Zr ($^{40}$Ca + $^{90}$Zr). This is because that the PQNT channels are opened in $^{32}$S ($^{40}$Ca) + $^{94,96}$Zr, c.f. the $Q$ values for neutron transfer listed in Table 1. We first perform the ECC calculations with couplings to the inelastic excitations channels considered only. The comparison of the results from ECC calculations to the experimental values for $^{32}$S + $^{94,96}$Zr and $^{40}$Ca + $^{94,96}$Zr is shown in Figure 3 by the dash lines. It can be seen that the experimental fusion data at near-barrier and sub-barrier energy show large enhancement as compared with the ECC calculations without the coupling to neutron transfer channels considered. Con-

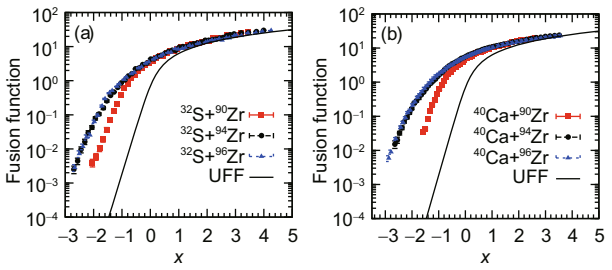


**Figure 1** (Color online) The reduced fusion function for reactions (a) $^{32}$S + $^{90,94,96}$Zr and (b) $^{40}$Ca + $^{90,94,96}$Zr as a function of $x$. The solid line represents the UFF. The experimental fusion cross sections are taken from refs. [38-41].

**Table 2** The barrier heights, radii, and curvatures used to reduce the fusion excitation functions

| Reaction | $V_B$ (MeV) | $\hbar\omega$ (MeV) | $R_B$ (fm) |
|---|---|---|---|
| $^{32}$S+$^{90}$Zr | 81.37 | 4.00 | 10.54 |
| $^{32}$S+$^{94}$Zr | 80.64 | 3.95 | 10.64 |
| $^{32}$S+$^{96}$Zr | 80.30 | 3.90 | 10.70 |
| $^{40}$Ca+$^{90}$Zr | 99.94 | 4.02 | 10.74 |
| $^{40}$Ca+$^{94}$Zr | 99.07 | 3.97 | 10.84 |
| $^{40}$Ca+$^{96}$Zr | 98.65 | 3.97 | 10.88 |

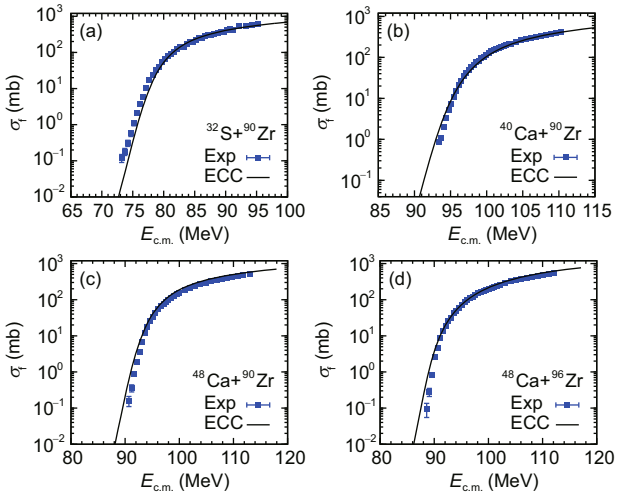


**Figure 2** (Color online) The calculated and experimental fusion excitation functions for the reactions (a) $^{32}$S+ $^{90}$Zr, (b) $^{40}$Ca + $^{90}$Zr, (c) $^{48}$Ca + $^{90}$Zr, and (d) $^{48}$Ca + $^{96}$Zr. The solid lines denote the results from the ECC calculations. The experimental fusion excitation functions are taken from refs. [38, 40, 69].

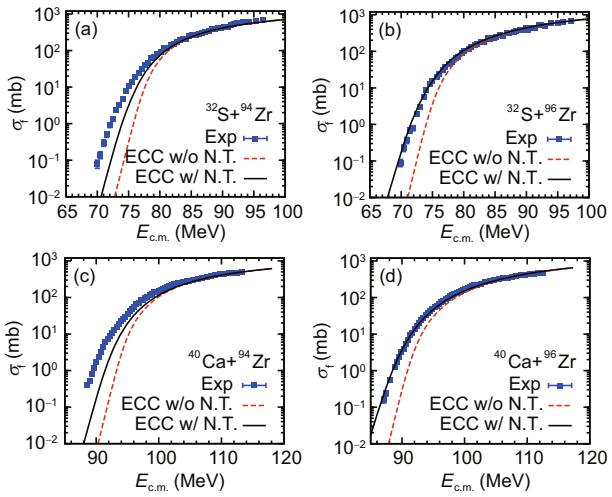


**Figure 3** (Color online) The calculated and experimental fusion excitation functions for reactions (a) $^{32}$S + $^{94}$Zr, (b) $^{32}$S + $^{96}$Zr, (c) $^{40}$Ca + $^{94}$Zr, and (d) $^{40}$Ca + $^{96}$Zr. The dash lines denote the results from the ECC calculations without the coupling to the neutron transfer channels considered. The solid lines denote the results from the ECC calculations with the coupling to the neutron transfer channels considered. The quadrupole deformation parameters of $\beta_2 = 0.062$ and $\beta_2 = 0.217$ are used for $^{94}$Zr and $^{96}$Zr [66], respectively. The experimental fusion excitation functions are taken from refs. [38-41].

sequently, these enhancements may be from the coupling to PQNT channels.

In the ECC model, the effect of coupling to the PQNT channels is simulated by broadening the barrier distribution which is related to the $Q(2n)$ value. The results from ECC calculations with the neutron transfer effects taken into account are shown in Figure 3 by the solid line. For $^{32}$S + $^{96}$Zr and $^{40}$Ca + $^{96}$Zr, it can be seen that the calculated results are in good agreement with the experimental values. But, for $^{32}$S + $^{94}$Zr and $^{40}$Ca + $^{94}$Zr, the calculated results underestimate the sub-barrier cross sections considerably. To understand this underestimation, we follow Jia et al. [41] and examine the relative enhancement. The relative enhancement is calculated as the ratio of the experimental fusion cross section to the calculated result by using the ECC model without the coupling to the neutron transfer channels considered, i.e., $f_{\rm R.E.} = \sigma^{\rm exp}(E_{\rm c.m.})/\sigma^{\rm th}_{\rm ECC}(E_{\rm c.m.})$. Figure 4 shows these relative enhancements for $^{32}$S + $^{94,96}$Zr and $^{40}$Ca + $^{94,96}$Zr. From Figures 4(a) and (b), one can find that the relative enhancements for the reactions with $^{94}$Zr as target are much larger than those for the reactions with $^{96}$Zr as target. This implies that if the estimates of the enhancement due to inelastic excitations channel couplings for the $^{32}$S + $^{94}$Zr and $^{40}$Ca + $^{94}$Zr are reliable, the effect of PQNT in $^{32}$S + $^{94}$Zr ($^{40}$Ca + $^{94}$Zr) is much stronger than that in $^{32}$S + $^{96}$Zr ($^{40}$Ca + $^{96}$Zr).

Next let's discuss the discrepancies between the calculated fusion cross sections and the experimental values from another viewpoint: We first estimate the effect of coupling to the PQNT channels, then constrain the coupling effects due to inelastic excitation channels. Within the ECC model, for $^{32}$S + $^{94,96}$Zr and $^{40}$Ca + $^{94,96}$Zr, the influence of neutron transfer should be almost the same because $Q(2n)$ values for these four reactions are very similar (see Table 1). As discussed in sect. 3.1, the total effect of the couplings to the inelastic excitations and neutron transfer channels in $^{32}$S + $^{94}$Zr ($^{40}$Ca + $^{94}$Zr) is also almost the same as that in $^{32}$S + $^{96}$Zr ($^{40}$Ca + $^{96}$Zr). Therefore the enhancement of the fusion cross section due to couplings to inelastic excitations channels in reactions with $^{94}$Zr and $^{96}$Zr should be similar to each other. This implies that the structure information related to fusion as described by the ECC model for $^{94}$Zr and $^{96}$Zr should be similar, i.e., the quadrupole deformation parameters $\beta_2$'s for $^{94}$Zr and $^{96}$Zr should be similar to each other in ECC calculations. In order to check this conjecture, we calculate the fusion cross sections with $\beta_2 = 0.217$ for $^{94}$Zr, the same as that of $^{96}$Zr. The results obtained from ECC calculations with the PQNT effect taken into account are shown in Figure 5. One can find

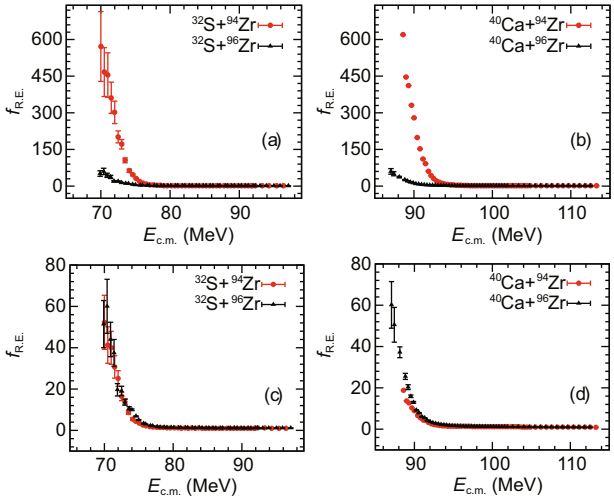


**Figure 4** (Color online) The relative enhancement $f_{\rm R.E.}$ owing to the coupling to PQNT channels for the reactions $^{32}$S + $^{94,96}$Zr ((a) and (c)) and $^{40}$Ca + $^{94,96}$Zr ((b) and (d)). The upper panels (a) and (b) show the results obtained with $\beta_2 = 0.062$ for $^{94}$Zr used and the lower panels (c) and (d) show the results obtained with $\beta_2 = 0.217$ for $^{94}$Zr used. The experimental fusion excitation functions are taken from refs. [38-41].

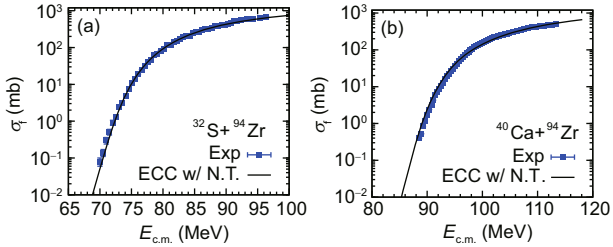


**Figure 5** (Color online) The calculated and experimental fusion excitation functions for the reactions (a) $^{32}$S + $^{94}$Zr and (b) $^{40}$Ca + $^{94}$Zr. The calculated fusion excitation functions are obtained from ECC calculations with the neutron transfer effects taken into account. The quadrupole deformation parameter $\beta_2 = 0.217$ for $^{94}$Zr is used. The solid squares denote the experimental values taken from refs. [39, 41].

that the calculated fusion cross sections are in good agreement with the data. In addition, as can be seen in Figures 4(c) and (d), the relative enhancements of the reactions with $^{94}$Zr as target are almost the same as those of the reactions with $^{96}$Zr as target.

### 3.3 The issue of quadrupole deformation for $^{94}$Zr

Within the ECC model [62], the formulas for calculating the parameters of the barrier distribution were proposed based on the quadrupole deformation parameters $\beta_2$ predicted by the FRDM [66]. According to the FRDM, $\beta_2 = 0.062$ for $^{94}$Zr and $\beta_2 = 0.217$ for $^{96}$Zr; they are quite different.

As discussed before, the total effect of couplings to inelastic excitations and neutron transfer channels on fusion in the reaction $^{32}$S + $^{94}$Zr ($^{40}$Ca + $^{94}$Zr) is almost the same as that in the reaction $^{32}$S + $^{96}$Zr ($^{40}$Ca + $^{96}$Zr). On one hand, according to the estimate of the enhancement due to inelastic excitations channel couplings obtained from ECC calculations with $\beta_2 = 0.062$ for $^{94}$Zr and $\beta_2 = 0.217$ for $^{96}$Zr, one may conclude that the role of PQNT channels in the reactions with $^{94}$Zr as target should be very different from that in the reactions with $^{96}$Zr as target. On the other hand, within the ECC model, the role of PQNT channels in $^{32}$S + $^{94,96}$Zr and $^{40}$Ca + $^{94,96}$Zr should be similar because the $Q(2n)$ values are similar in these four reactions. This implies that the quadrupole deformation parameters of $^{94}$Zr and $^{96}$Zr should be similar to each other. Indeed, if one assumes that the quadrupole deformation parameter of $^{94}$Zr is the same as that of $^{96}$Zr, i.e., $\beta_2 = 0.217$, the fusion cross sections for reactions with $^{94}$Zr as target from the ECC model are in good agreement with the experiment (see Figure 5).

Therefore, it becomes a puzzling issue whether the quadrupole deformation parameters for $^{94}$Zr and $^{96}$Zr are similar to each other or not. In Table 3 we present $\beta_2$ values of $^{94}$Zr and $^{96}$Zr given in refs. [74, 75]. The quadrupole deformation parameters deduced from $B(E2; \text{g.s.} \rightarrow 2_1^+)$ for $^{94}$Zr and $^{96}$Zr are quite small, but very close to each other, $\beta_2(^{94}\text{Zr}) = 0.09$ and $\beta_2(^{96}\text{Zr}) = 0.08$ [74]. In ref. [75], a relativistic mean-field model was adopted to study the structural evolution in transition nuclei including $^{94}$Zr and $^{96}$Zr. With the NL3 interaction, the obtained $\beta_2$'s for $^{94}$Zr and $^{96}$Zr are 0.169 and 0.243, which are also similar. However, with the NL3* interaction, the obtained $\beta_2$'s for $^{94}$Zr and $^{96}$Zr are 0.002 and 0.233, which are quite different.

To solve this puzzling issue and get further understanding of the coupling to PQNT channels, we suggest to measure the fusion excitation function of the reactions $^{48}$Ca + $^{94}$Zr or $^{36}$S + $^{94}$Zr. In these two reactions, the PQNT channels are closed (see Table 1). Therefore, these two reactions can be used to test the structure information connected to fusion of the target $^{94}$Zr. If the results obtained from ECC calculations together with the quadrupole deformation parameters predicted from FRDM are in good agreement with the measured fusion excitation functions, one can conclude that the influence of PQNT channel coupling on sub-barrier fusion cross section in the reaction $^{32}$S + $^{94}$Zr ($^{40}$Ca + $^{94}$Zr) is stronger than that in the reaction $^{32}$S + $^{96}$Zr ($^{40}$Ca + $^{96}$Zr). Otherwise, further study of the structure related to fusion of $^{94}$Zr are needed. In any case, we can get a better understanding of the coupling to PQNT channels.

**Table 3** The quadrupole deformation parameters for $^{94}$Zr and $^{96}$Zr

| $\beta_2$ | FRDM [66] | RMF (NL3) [75] | RMF (NL3*) [75] | Expt. [74] |
|---|---|---|---|---|
| $^{94}$Zr | 0.062 | 0.169 | 0.002 | 0.09 |
| $^{96}$Zr | 0.217 | 0.243 | 0.233 | 0.08 |

## 4 Summary

In summary, we adopt the universal fusion function formalism and the ECC model to investigate the dynamic coupling effects on fusion cross sections for the reactions $^{32}$S + $^{94,96}$Zr and $^{40}$Ca + $^{94,96}$Zr. The reduced fusion excitation functions show that the total effect of inelastic excitations and neutron transfer channel couplings on fusion in $^{32}$S + $^{94}$Zr ($^{40}$Ca + $^{94}$Zr) is almost the same as that in $^{32}$S + $^{96}$Zr ($^{40}$Ca + $^{96}$Zr). Within the ECC model, the enhancements due to inelastic excitations channel couplings and neutron transfer channel coupling are evaluated separately. The results show that influences of neutron transfer in the reactions with $^{94}$Zr as target should be almost the same as that in the reactions with $^{96}$Zr as target. This implies that the quadrupole deformation parameters of $^{94}$Zr and $^{96}$Zr should be similar to each other. However, the quadrupole deformation parameters predicted from FRDM used in the ECC model are quite different. Experiments on $^{48}$Ca + $^{94}$Zr or $^{36}$S + $^{94}$Zr are suggested to solve the puzzling issue of whether the quadrupole deformation parameters for $^{94}$Zr and $^{96}$Zr are similar to each other or not.

*This work was supported by the National Key Basic Research Program of China (Grant No. 2013CB834400), the National Natural Science Foundation of China (Grant Nos. 11175252, 11120101005, 11275248, 11475115, and 11525524) and the Knowledge Innovation Project of the Chinese Academy of Sciences (Grant No. KJCX2-EW-N01). The computational results presented in this work have been obtained on the High-performance Computing Cluster of SKLTP/ITP-CAS and the ScGrid of the Supercomputing Center, Computer Network Information Center of the Chinese Academy of Sciences.*

1 A. B. Balantekin, and N. Takigawa, Rev. Mod. Phys. **70**, 77 (1998).
2 M. Dasgupta, D. J. Hinde, N. Rowley, and A. M. Stefanini, Annu. Rev. Nucl. Part. Sci. **48**, 401 (1998).
3 M. S. Hussein, L. F. Canto, P. R. S. Gomes, and R. Donangelo, Phys. Rep. **424**, 1 (2006).
4 B. B. Back, H. Esbensen, C. L. Jiang, and K. E. Rehm, Rev. Mod. Phys. **86**, 317 (2014).
5 U. G. Meißner, Sci. Bull. **60**, 43 (2014).
6 L. F. Canto, P. R. S. Gomes, R. Donangelo, J. Lubian, and M. S. Hussein, Phys. Rep. **596**: 1 (2015).

7 C. B. Fu, J. Bao, L. M. Chen, J. J. He, L. Hou, L. Li, Y. F. Li, Y. T. Li, G. Q. Liao, Y. Rhee, Y. Sun, S. W. Xu, D. W. Yuan, X. P. Zhang, G. Zhao, J. R. Zhao, B. J. Zhu, J. Q. Zhu, and J. Zhang, Sci. Bull. **60**, 1211 (2015).

8 G. G. Adamian, N. V. Antonenko, and W. Scheid, Nucl. Phys. A **618**, 176 (1997).

9 G. G. Adamian, N. V. Antonenko, W. Scheid, and V. V. Volkov, Nucl. Phys. A **633**, 409 (1998).

10 G. G. Adamian, N. V. Antonenko, and Y. M. Tchuvil'sky, Phys. Lett. B **451**, 289 (1999).

11 G. N. Knyazheva, E. M. Kozulin, R. N. Sagaidak, A. Y. Chizhov, M. G. Itkis, N. A. Kondratiev, V. M. Voskressensky, A. M. Stefanini, B. R. Behera, L. Corradi, E. Fioretto, A. Gadea, A. Latina, S. Szilner, M. Trotta, S. Beghini, G. Montagnoli, F. Scarlassara, F. Haas, N. Rowley, P. R. S. Gomes, and A. S. de Toledo, Phys. Rev. C **75**, 064602 (2007).

12 N. Wang, E. G. Zhao, W. Scheid, and S. G. Zhou, Phys. Rev. C **85**, 041601(R) (2012).

13 N. Wang, E. Zhao, and S. G. Zhou, J. Phys.-Conf. Ser. **515**, 012022 (2014).

14 J. Zhang, C. Wang, and Z. Ren, Nucl. Phys. A **909**, 36 (2013).

15 J. J. Shen, and C. W. Shen, Sci. China-Phys. Mech. Astron. **57**, 453 (2014).

16 X. H. Fan, J. M. Dong, and W. Zuo, Sci. China-Phys. Mech. Astron. **58**, 062002 (2015).

17 Q. H. Mo, M. Liu, L. C. Cheng, and N. Wang, Sci. China-Phys. Mech. Astron. **58**, 082001 (2015).

18 C. L. Jiang, H. Esbensen, K. E. Rehm, B. B. Back, R. V. Janssens, J. A. Caggiano, P. Collon, J. Greene, A. M. Heinz, D. J. Henderson, I. Nishinaka, T. O. Pennington, and D. Seweryniak, Phys. Rev. Lett. **89**, 052701 (2002).

19 S. Misicu, H. Esbensen. Phys. Rev. Lett. **96**, 112701 (2006).

20 M. Dasgupta, D. J. Hinde, A. Diaz-Torres, B. Bouriquet, C. I. Low, G. J. Milburn, and J. O. Newton, Phys. Rev. Lett. **99**, 192701 (2007).

21 A. Diaz-Torres, D. Hinde, M. Dasgupta, G. J. Milburn, and J. A. Tostevin, Phys. Rev. C **78**, 064604 (2008).

22 T. Ichikawa, K. Hagino, and A. Iwamoto, Phys. Rev. Lett. **103**, 202701 (2009).

23 V. Y. Denisov, Phys. Rev. C **89**, 044604 (2014).

24 P. R. S. Gomes, R. Linares, J. Lubian, C. C. Lopes, E. N. Cardozo, B. H. F. Pereira, and I. Padron, Phys. Rev. C **84**, 014615 (2011).

25 V. V. Sargsyan, G. G. Adamian, N. V. Antonenko, W. Scheid, and H. Q. Zhang, Phys. Rev. C **86**, 054610 (2012).

26 L. R. Gasques, D. J. Hinde, M. Dasgupta, A. Mukherjee, and R. G. Thomas, Phys. Rev. C **79**, 034605 (2009).

27 M. Dasgupta, L. R. Gasques, D. H. Luong, R. du Rietz, R. Rafiei, D. J. Hinde, C. J. Lin, M. Evers, and A. Diaz-Torres, Nucl. Phys. A **834**, 147c (2010).

28 M. Beckerman, M. Salomaa, A. Sperduto, H. Enge, J. Ball, A. DiRienzo, S. Gazes, Y. Chen, J. D. Molitoris, and N. Mao, Phys. Rev. Lett. **45**, 1472 (1980).

29 R. A. Broglia, C. H. Dasso, S. Landowne, and A. Winther, Phys. Rev. C **27**, 2433 (1983).

30 R. A. Broglia, C. H. Dasso, S. Landowne, and G. Pollarolo, Phys. Lett. B **133**, 34 (1983).

31 P. H. Stelson, H. J. Kim, M. Beckerman, D. Shapira, and R. L. Robinson, Phys. Rev. C **41**, 1584 (1990).

32 C. H. Dasso, S. Landowne, and A. Winther, Nucl. Phys. A **405**, 381 (1983).

33 C. H. Dasso, S. Landowne, and A. Winther, Nucl. Phys. A **407**, 221 (1983).

34 G. L. Zhang, X. X. Liu, and C. J. Lin, Phys. Rev. C **89**, 054602 (2014).

35 B. Wang, W. J. Zhao, P. R. S. Gomes, E. G. Zhao, and S. G. Zhou, Phys. Rev. C **90**, 034612 (2014).

36 R. Pengo, D. Evers, K. E. G. Löbner, U. Quade, K. Rudolph, S. J. Skorka, and I. Weidl, Nucl. Phys. A **411**, 255 (1983).

37 H. A. Aljuwair, R. J. Ledoux, M. Beckerman, S. B. Gazes, J. Wiggins, E. R. Cosman, R. R. Betts, S. Saini, and O. Hansen, Phys. Rev. C **30**, 1223 (1984).

38 H. Timmers, D. Ackermann, S. Beghini, L. Corradi, J. H. He, and G. Montagnoli, Nucl. Phys. A **633**, 421 (1998).

39 M. Trotta, S. Szilner, F. Scarlassara, N. Rowley, G. Montagnoli, A. Gadea, E. Fioretto, L. Corradi, S. Beghini, B. R. Behera, and A. M. Stefanini, Phys. Rev. C **76**, 014610 (2007).

40 H. Q. Zhang, C. J. Lin, F. Yang, H. M. Jia, X. Xu, and Z. D. Wu, Phys. Rev. C **82**, 054609 (2010).

41 H. M. Jia, C. J. Lin, F. Yang, X. X. Xu, H. Q. Zhang, Z. H. Liu, Z. D. Wu, L. Yang, N. R. Ma, P. F. Bao, and L. J. Sun, Phys. Rev. C **89**, 064605 (2014).

42 P. Jacobs, Z. Fraenkel, G. Mamane, and I. Tserruya, Phys. Lett. B **175**, 271 (1986).

43 H. M. Jia, C. J. Lin, F. Yang, X. X. Xu, H. Q. Zhang, Z. H. Liu, L. Yang, S. T. Zhang, P. F. Bao, and L. J. Sun, Phys. Rev. C **86**, 044621 (2012).

44 V. I. Zagrebaev, Phys. Rev. C **67**, 061601(R) (2003).

45 V. V. Sargsyan, G. G. Adamian, N. V. Antonenko, W. Scheid, and H. Q. Zhang, Phys. Rev. C **86**, 014602 (2012).

46 V. V. Sargsyan, G. Scamps, G. G. Adamian, N. V. Antonenko, and D. Lacroix, Phys. Rev. C **88**, 064601 (2013).

47 V. V. Sargsyan, G. G. Adamian, N. V. Antonenko, W. Scheid, and A. H. Q. Zhang, Phys. Rev. C **91**, 014613 (2015).

48 K. Hagino, N. Rowley, and A. T. Kruppa, Comput. Phys. Commun. **123**, 143 (1999).

49 N. Wang, Z. Li, and X. Wu, Phys. Rev. C **65**, 064608 (2002).

50 N. Wang, K. Zhao, and Z. Li, Phys. Rev. C **90**, 054610 (2014).

51 N. Wang, Z. Li, X. Wu, J. Tian, Y. Zhang, and M. Liu, Phys. Rev. C **69**, 034608 (2004).

52 K. Wen, F. Sakata, Z. X. Li, X. Z. Wu, Y. X. Zhang, and S. G. Zhou, Phys. Rev. Lett. **111**, 012501 (2013).

53 K. Wen, F. Sakata, Z. X. Li, X. Z. Wu, Y. X. Zhang, and S. G. Zhou, Phys. Rev. C **90**, 054613 (2014).

54 N. Wang, K. Zhao, and Z. X. Li, Sci. China-Phys. Mech. Astron. **58**, 112001 (2015).

55 A. S. Umar, and V. E. Oberacker, Phys. Rev. C **74**, 021601(R) (2006).

56 A. S. Umar, V. E. Oberacker, J. A. Maruhn, and P.-G. Reinhard, Phys. Rev. C **85**, 017602 (2012).

57 R. Keser, A. S. Umar, and V. E. Oberacker, Phys. Rev. C **85**, 044606 (2012).

58 L. Guo, J. A. Maruhn, and P. G. Reinhard, Phys. Rev. C, **76**, 014601 (2007).

59 L. Guo, J. A. Maruhn, P. G. Reinhard, and Y. Hashimoto, Phys. Rev. C **77**, 041301(R) (2008).

60 G. F. Dai, L. Guo, E. G. Zhao, and S. G. Zhou, Sci. China-Phys. Mech.

Astron. **57**, 1618 (2014).

61 G. F. Dai, L. Guo, E. G. Zhao, and S. G. Zhou, Phys. Rev. C **90**, 044609 (2014).

62 B. Wang, K. Wen, W. J. Zhao, E. G. Zhao, and S. G. Zhou, arXiv:1504.00756.

63 B. Wang, W. J. Zhao, A. Diaz-Torres, E. G. Zhao, and S. G. Zhou, Phys. Rev. C **93**, 014615 (2016).

64 D. L. Hill, and J. A. Wheeler, Phys. Rev. **89**, 1102 (1953).

65 L. L. Li, S. G. Zhou, E. G. Zhao, and W. Scheid, Int. J. Mod. Phys. E **19**, 359 (2010).

66 P. Möller, J. R. Nix, W. D. Myers, and W. J. Swiatecki, At. Data Nucl. Data Tables **59**, 185 (1995).

67 L. F. Canto1, P. R. S. Gomes, J. Lubian, L. C. Chamon, and E. Crema, J. Phys. G-Nucl. Part. Phys. **36**, 015109 (2009).

68 L. F. Canto, P. R. S. Gomes, J. Lubian, L. C. Chamon, and E. Crema, Nucl. Phys. A **821**, 51 (2009).

69 A. M. Stefanini, F. Scarlassara, S. Beghini, G. Montagnoli, R. Silvestri, M. Trotta, B. R. Behera, L. Corradi, E. Fioretto, A. Gadea, Y. W. Wu, S. Szilner, H. Q. Zhang, Z. H. Liu, M. Ruan, F. Yang, and N. Rowley, Phys. Rev. C **73**, 034606 (2006).

70 M. A. C. Ribeiro, L. C. Chamon, D. Pereira, M. S. Hussein, and D. Galetti, Phys. Rev. Lett. **78**, 3270 (1997).

71 L. C. Chamon, D. Pereira, M. S. Hussein, M. A. C. Ribeiro, and D. Galetti, Phys. Rev. Lett. **79**, 5218 (1997).

72 L. C. Chamon, B. V. Carlson, L. R. Gasques, D. Pereira, C. De Conti, and M. S. G. Alvares, Phys. Rev. C **66**, 014610 (2002).

73 C. Y. Wong, Phys. Rev. Lett. **31**, 766 (1973).

74 S. Raman, C. W. Nestor, and P. Tikkanen, At. Data Nucl. Data Tables **78**, 1 (2001).

75 M. Bhuyan, Phys. Rev. C **92**, 034323 (2015).